Anisotropic flow fluctuations in Pb+Pb collisions at LHC

L.V Bravina[2,3,4,a], E.S. Fotina[1], V.L. Korotkikh[1], I.P. Lokhtin[1], L.V. Malinina[1,5], E.N. Nazarova[1], S.V. Petrushanko[1], A.M. Snigirev[1], and E.E. Zabrodin[1,2,3,4]

[1] *Skobeltsyn Institute of Nuclear Physics, Moscow State University, RU-119991 Moscow, Russia*

[2] *Department of Physics, University of Oslo, PB 1048 Blindern, Oslo, Norway*

[3] *Frankfurt Institute for Advanced Studies, Ruth-Moufang-Str. 1, 60438 Frankfurt a.M., Germany*

[4] *National Research Nuclear University "MEPhI" (Moscow Engineering Physics Institute), RU-115409 Moscow, Russia*

[5] *Joint Institute for Nuclear Researches, Dubna, Russia*

Abstract. Fluctuations of anisotropic flow in lead-lead collisions at LHC energies arising in HYDJET++ model are studied. It is shown that intrinsic fluctuations of the flow which appear mainly because of the fluctuations of particle multiplicity, momenta and coordinates are insufficient to match the measured experimental data, provided the eccentricity of the freeze-out hypersurface is fixed at any given impact parameter b. However, when the variations of the eccentricity in HYDJET++ are taken into account, the agreement between the model results and the data is drastically improved. Both model calculations and the data are filtered through the unfolding procedure. This procedure eliminates the non-flow fluctuations to a higher degree, thus indicating a dynamical origin of the flow fluctuations in HYDJET++ event generator.

1 Introduction

Anisotropic flow of secondary particles in ultra-relativistic heavy-ion collisions is very sensitive to creation of even a small amount of quark-gluon plasma (QGP). This topic is a quickly developing branch of modern high energy physics. The present status of the theory and the experiment can be found, e.g., in topical reviews [1–7] and references therein. To analyse the flow the particle distribution in azimuthal plane is decomposed into the Fourier series [8, 9]

$$\frac{dN}{d\phi} \quad \propto \quad 1 + 2 \sum_{n=1}^{\infty} v_n(p_T) \cos\left[n(\phi - \Psi_n)\right] \tag{1}$$

$$v_n \quad = \quad \langle \cos\left[(n(\phi - \Psi_n)]\right\rangle , \tag{2}$$

with p_T, ϕ and Ψ_n being the particle transverse momentum, the particle azimuthal angle and the azimuth of the participant plane of n-th order, respectively. The Fourier harmonics v_n are called directed flow (v_1), elliptic flow (v_2), triangular flow (v_3), quadrangular flow (v_4) and so forth. As a collective effect, the flow is nicely described by hydrodynamic models [10] (see, however, [11]), although the p_T-distributions of the flow harmonics are usually traced to transverse momenta $p_T \simeq 2$ GeV/c, and hard

---

[a] e-mail: larissa.bravina@fys.uio.no

processes are not considered. The HYDJET++ model [12–14], in contrast, combines parametrised hydrodynamic treatment of soft processes with the description of hard jets traversing hot and dense partonic medium. The interplay between soft hydro-like processes and jets within the HYDJET++ was studied in a number of papers [15–23]. The model predicted correctly violation of the number-of-constituent-quark (NCQ) scaling of v_2 at LHC, whereas the scaling certainly holds for hadrons produced in soft processes [15, 16], rise of the high-p_T tail of $v_4(p_T)/v_2^2(p_T)$ ratio [17, 18], the important role of elliptic and triangular flow non-linear contributions to higher order harmonics [14, 19–21] and to the long-range angular di-hadron correlations leading to the formation of characteristic "ridge" structures [22]. Our recent study [23] was devoted to event-by-event (EbyE) fluctuations which alter the resulting anisotropic flow. To what extent these fluctuations are taken into account in the HYDJET++? - The answer to this question is given below. Section 2 presents basic principles of the anisotropic flow generation in the model.

2 Generation of anisotropic flow in HYDJET++

Detailed description of the event generator HYDJET++, which merges thermalized hydro-like state with separated chemical and thermal freeze-outs [24, 25] with in-medium fragmentation of hard partons [26], can be found elsewhere [12]. The fine tuning of free model parameters was done in [13] to match the bulk observables in lead-lead collisions at LHC. Implementation of triangular flow in addition to the elliptic one provided the possibility to describe the basic features of higher flow harmonics up to hexagonal flow [14, 21]. This is done in a straightforward manner. Namely, the elliptic spatial deformation of the freeze-out hypersurface depends on the spatial anisotropy parameter $\varepsilon(b)$, where b is the impact parameter, as [25]

$$R_{ell}(b, \varphi) = R_{fo}(b) \sqrt{\frac{1 - \varepsilon^2(b)}{1 + \varepsilon(b) \cos 2\varphi}} \tag{3}$$

Here parameter $R_{fo}(b) = R_0 \sqrt{1 - \varepsilon(b)}$ determines the scale of the transverse size of the fireball at freeze-out and φ is the azimuthal angle between the transverse velocity of the fluid element and the impact parameter axis. In contrast to transverse isotropic parametrisation, the angle φ in HYDJET++ does not coincide with the azimuthal angle ϕ but is linked to it via the nonzero flow anisotropy parameter $\delta(b)$

$$\tan \varphi = \sqrt{\frac{1 - \delta(b)}{1 + \delta(b)}} \tan \phi \tag{4}$$

Both parameters $\varepsilon(b)$ and $\delta(b)$ are proportional to the initial spatial anisotropy $\varepsilon_0 = b/(2R_A)$.

To extend the model to triangular flow, triangular deformations should be included [14]

$$R_{triang}(b, \varphi) = R_{ell}(b, \varphi)\{1 + \varepsilon_3(b) \cos [3(\varphi - \Psi_3)]\} . \tag{5}$$

Since no correlations between the reaction planes of elliptic and triangular flows are observed, i.e. $v_2(\Psi_3) = v_3(\Psi_2) \equiv 0$, the azimuth Ψ_3 is randomly generated, while Ψ_2 is always set to zero in model calculations. A new free parameter $\varepsilon_3(b)$ entering Eq. (5) controls the degree of triangularity of the system. It is important to stress that, although the three parameters $\varepsilon(b)$, $\delta(b)$ and $\varepsilon_3(b)$ were up to recent times fixed in the model, e.g., $\varepsilon_3(b_1) = \varepsilon_3(b_2)$ if $b_1 = b_2$, the flow harmonics $v_n(p_T)$ must be obtained only after averaging over a sample of generated events due to event-by-event fluctuations. The flow fluctuations in HYDJET++ arise because of (i) fluctuations in particle multiplicity, (ii) fluctuations in particle coordinates and directly linked to it (iii) fluctuations in particle momenta (via the correlations with radial flow), (iv) decays of resonances, and (v) production of (mini)jets. These fluctuations are investigated in Sec. 3.
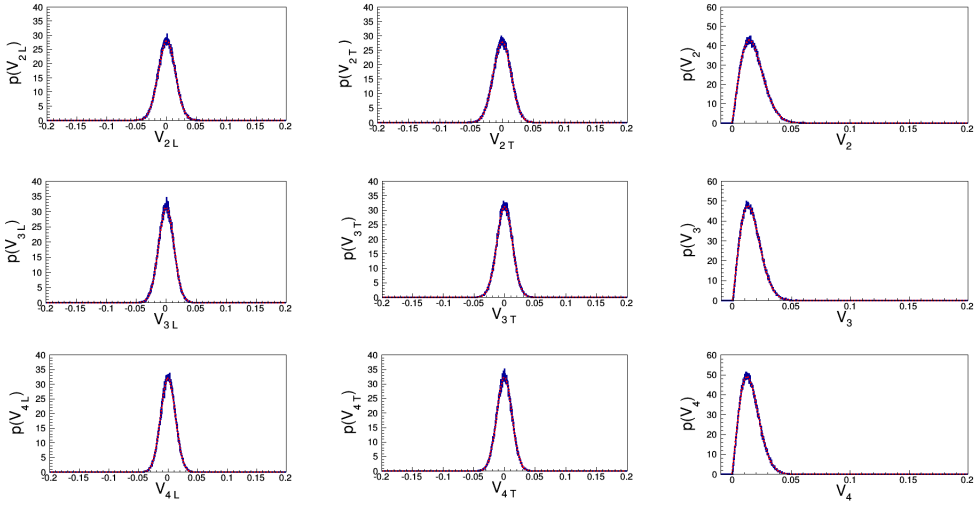
Figure 1. The probability density distributions for V_{nL} (left column), V_{nT} (middle column), and for the modulus of the flow vector $V_n = |\vec{V}_n|$, $n = 2, 3, 4$ (right column) for central Pb+Pb collisions in HYDJET++ with $b = 0$. Dashed red curves in the plots indicate the fit of simulated HYDJET++ points to Eq. (6) (left), Eq. (7) (middle) and Eq. (8) (right), respectively.

3 Event-by-event flow in HYDJET++

Let us determine the flow vector $\vec{V}_n$ and its modulus $V_n = \vec{V}_n$, $n = 2, 3, 4$ in a single event. - From here we use capital letters to distinguish the components of EbyE-determined flow vector $\vec{V}_n$ from the flow harmonics v_n, obtained after averaging of $\cos[n(\varphi - \Psi_n)]$ over all particles in all events. - Since we know the direction of the "true" vector $\vec{V}_n$ for a given event with the impact parameter b in model calculations, it is possible to decompose the obtained flow vector into longitudinal part $\vec{V}_{nL}$, which is parallel to the direction of the "true" vector, and the transverse part $\vec{V}_{nT}$ perpendicular to it.

Firstly, one has to study the intrinsic fluctuations in HYDJET++ arising in a system when the anisotropic flow is absent. This situation corresponds to the case of perfect central collisions with zero impact parameter. The all three parameters are zero, $\varepsilon(0) = \delta(0) = \varepsilon_3(0) = 0$, and the probability distributions for both EbyE flow components, $\vec{V}_{nL}$ and $\vec{V}_{nT}$, and the modulus V_n should be represented by Gaussian functions [27, 28]

$$P(\vec{V}_{nL}) = \frac{1}{2\pi\sigma_n^2(0)} \exp\left[-\frac{\vec{V}_{nL}^2}{2\sigma_n^2(0)}\right], \tag{6}$$

$$P(\vec{V}_{nT}) = \frac{1}{2\pi\sigma_n^2(0)} \exp\left[-\frac{\vec{V}_{nT}^2}{2\sigma_n^2(0)}\right], \tag{7}$$

$$P(V_n) = \frac{V_n}{\sigma_n^2(0)} \exp\left[-\frac{V_n^2}{2\sigma_n^2(0)}\right]. \tag{8}$$
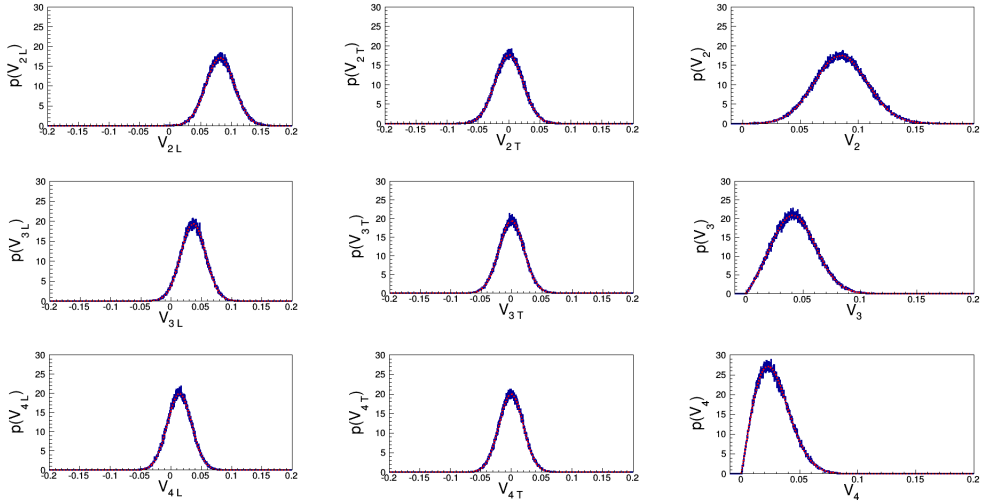
Figure 2. The same as Fig. 1 but for 20-25% centrality collisions. Dashed red curves in the plots indicate the fit of simulated HYDJET++ points to Eq. (9) (left), Eq. (10) (middle) and Eq. (11) (right), respectively.

The results of model calculations fitted to Eqs.(6)-(8) are displayed in Fig. 1. One may see that the simulated distributions and the fit are on the top of each other. Both longitudinal and transverse distributions of the flow vector are symmetric with respect to zero, meaning that the event-integrated flow is essentially zero. Note, that for any *n*-th component of the flow vector all Gaussians depend on a single parameter σ_n. For instance, the modulus mean is $\langle V_n \rangle = \sqrt{\frac{\pi}{2}} \, \sigma_n$, whereas the width of the $P(V_n)$ distribution reads $\sigma_{V_n} = \sqrt{2 - \frac{\pi}{2}} \, \sigma_n$. As seen in Fig. 1, the parameter σ_n is almost the same for all three components, $\sigma_2 \approx \sigma_3 \approx \sigma_4 = 0.013$. Although σ_n depends on a number of model parameters, it is especially sensitive to the mean multiplicity, which controls the centrality variation of σ_n.

The case of collisions with non-zero impact parameters is a bit more complex. For these collisions the probability distributions given by Eqs.(6)-(8) should be modified accordingly [27, 28]

$$P(V_{nL}) = \frac{1}{\sqrt{2\pi\sigma_n^2(b)}} \exp\left[-\frac{(V_{nL} - \langle V_{nL} \rangle)^2}{2\sigma_n^2(b)} \right] , \qquad (9)$$

$$P(V_{nT}) = \frac{1}{\sqrt{2\pi\sigma_n^2(b)}} \exp\left[-\frac{(V_{nT})^2}{2\sigma_n^2(b)} \right] , \qquad (10)$$

$$P(V_n) = \frac{V_n}{\sigma_n^2(b)} \exp\left[-\frac{V_n^2 + \langle V_{nL} \rangle^2}{2\sigma_n^2(b)} \right] I_0\left(\frac{V_n \langle V_{nL} \rangle}{\sigma_n^2(b)} \right) , \qquad (11)$$

where I_0 is the modified Bessel function of the first kind. The probability densities of the components and modulus of the flow vector, calculated in lead-lead collisions with centrality 20-25%, are shown in Fig. 2. Results of the fit to Eqs.(9)-(11) are plotted onto the generated distributions as well. Several features should be mentioned here. The width σ_{V_n} and the average modulus $\langle V_n \rangle$ now depend on both

$\sigma_n(b)$ and $\langle V_{nL} \rangle$. Also note that $\langle V_n \rangle \neq \langle V_{nL} \rangle$ although $\langle V_{nL} \rangle = v_n(b)$, $n = 2, 3$, because the values of free parameters $\varepsilon(b)$, $\varepsilon_3(b)$, $\delta(b)$, responsible for emergence of spatial and momentum anisotropy in the model, are tuned to provide the correct description of elliptic and triangular flow at given impact parameter b. Then, the EbyE flow distributions at non-zero impact parameter, shown in Fig. 2, are broader compared to that at $b = 0$, presented in Fig. 1, but the widths of the longitudinal and transverse parts are still almost equal, $\sigma_2 \simeq \sigma_3 \simeq \sigma_4 = 0.02$. The values of V_{nL} at which $P(V_{nL})$ reach their maxima become smaller with rising harmonic number n thus reflecting the fact that $v_4 < v_3 < v_2$ at this centrality.

We demonstrated that event-by-event flow fluctuations arise in the model even when the parameters, responsible for the creation of spatial anisotropy, are fixed. The next step is the comparison of intrinsic EbyE fluctuations in HYDJET++ with the experimentally measured ones. This non-trivial problem is considered in Sec. 4.

4 Unfolding procedure and comparison with data

The EbyE distributions of harmonics of anisotropic flow in lead-lead collisions at LHC were studied, e.g., by ATLAS Collaboration in [29]. However, the results were obtained after the application of the so-called *unfolding* procedure in order to extract the "true" value of the flow vector and get rid of the non-flow effects caused by the finite event multiplicities, jet fragmentation and decays of resonances. The procedure is cumbersome, so often people simply rescale their predictions [30, 31] to make a comparison with the data. Analysis below shows that such a simplistic approach is not always justified. Let us consider implementation of the unfolding procedure in details.

As an input, one selects the spectra of charged particles with $p_T \geq 0.5$ GeV/c and $|\eta| < 2.5$, corresponding to ATLAS transverse momentum and pseudorapidity cuts. Angular distribution of particles is modified as

$$\frac{dN}{d\varphi} \propto 1 + 2 \sum_{n=1}^{\infty} V_n^{\mathrm{obs}} \cos\left[n(\varphi - \Psi_n^{\mathrm{obs}})\right] = 1 + 2 \sum_{n=1}^{\infty} \left(V_{n,x}^{\mathrm{obs}} \cos n\varphi + V_{n,y}^{\mathrm{obs}} \sin n\varphi\right), \qquad (12)$$

with V_n^{obs} being the magnitude of the observed per-particle flow vector, whereas Ψ_n^{obs} represents the azimuth of the event plane.

Then, the single-particle event-by-event distributions are constructed

$$\begin{aligned}
V_n^{\mathrm{obs}} &= \sqrt{(V_{n,x}^{\mathrm{obs}})^2 + (V_{n,y}^{\mathrm{obs}})^2}, \\
V_{n,x}^{\mathrm{obs}} &= V_n^{\mathrm{obs}} \cos n\Psi_n^{\mathrm{obs}} = \langle \cos n\varphi \rangle, \\
V_{n,y}^{\mathrm{obs}} &= V_n^{\mathrm{obs}} \sin n\Psi_n^{\mathrm{obs}} = \langle \sin n\varphi \rangle.
\end{aligned} \qquad (13)$$

Note, that the final "unfolded" distribution is insensitive to the method used for the extraction of the magnitude of the observed per-particle vector V_n^{obs} [29]. The two sub-events (2SE) method subdivides the event sample further into two sub-groups containing charged particles emitted in (i) forward and (ii) backward hemisphere in the c.m. system. The difference between the EbyE flow vectors of the two sub-events is fitted to the Gaussian with the width $\delta_{\mathrm{2SE}} = 2\delta$, which enters the response function [29]

$$P(V_n^{\mathrm{obs}}|V_n) \propto V_n^{\mathrm{obs}} \exp\left[-\frac{(V_n^{\mathrm{obs}})^2 + V_n^2}{2\delta^2}\right] I_0\left(\frac{V_n^{\mathrm{obs}} V_n}{\delta^2}\right). \qquad (14)$$
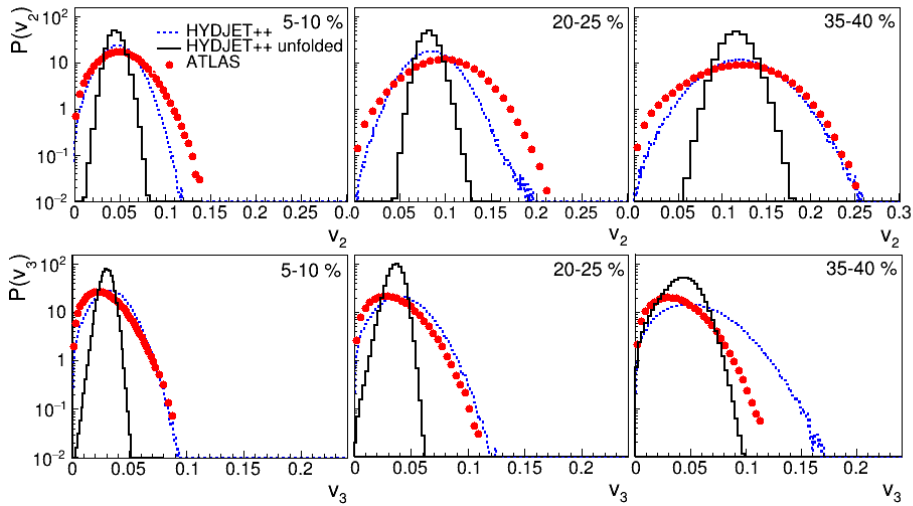
Figure 3. The probability density distributions of elliptic flow V_2 (upper row) and triangular flow V_3 (bottom row) in three centrality intervals: $5-10\%$ (left), $20-25\%$ (middle) and $35-40\%$ (right). Dashed and solid histograms present the results for simulated HYDJET++ events before and after the unfolding procedure, respectively. The full circles are the ATLAS data from [29].

The obtained response function is used then as an input to find the Bayesian unfolding matrix via the iteration procedure [32]. The contributions arising mostly due to non-flow processes and effects of finite particle multiplicity can be subtracted by the EbyE unfolding procedure in order to get the dynamical flow fluctuations only. How does it work?

Figure 3 displays the probability density distributions of elliptic and triangular EbyE flows obtained in three centrality intervals: $\sigma/\sigma_{geo} = 5-10\%$, $20-25\%$, and $35-40\%$ in the version of HYDJET++ with unsmeared eccentricity parameters. At first glance, the model results shown by dashed curves are not far from the ATLAS data. However, the experimental results are obtained by means of the unfolding procedure. It is unfolding that makes the HYDJET++ distributions much narrow, see solid histograms in Fig. 3, thus meaning that the dynamical fluctuations in the model are not strong enough to match the data.

The situation is changed dramatically if we allow for variations of $\varepsilon(b)$ and $\varepsilon_3(b)$. Now the values of both parameters are not fixed anymore but rather smeared normally around the unsmeared values with the widths proportional to these values. The proportionality coefficients are tuned to fit the data at a single arbitrary centrality, say $10-15\%$ or $20-25\%$, and the found values are used then for all other centralities.

Results obtained in HYDJET++ with the smeared anisotropy parameters are shown in Fig. 4. Now the initial $P(V_n)$ distributions are broader than the unfolded ones only in the areas of relatively high flow values. The agreement of unfolded spectra with the data is very good. Since unfolding suppresses strongly the non-flow fluctuations, both Fig. 3 and Fig. 4 indicate the dynamical origin of the flow fluctuations in HYDJET++.
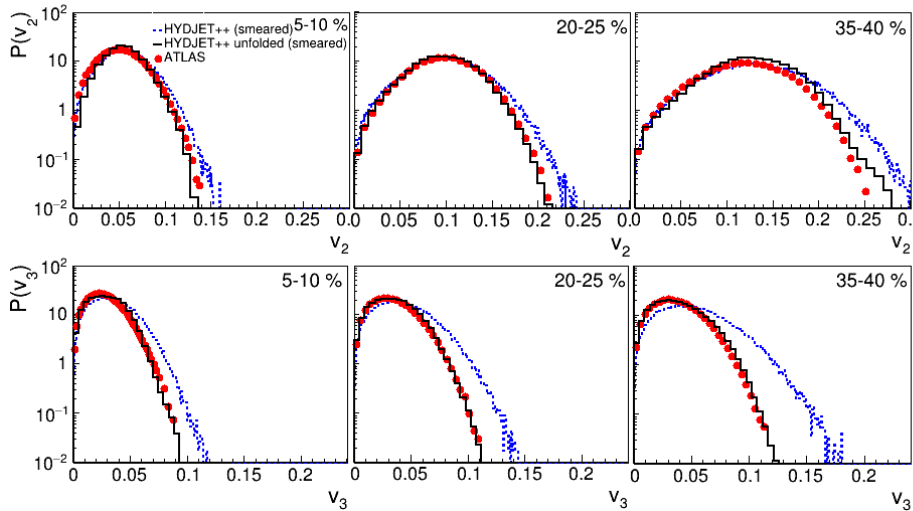
Figure 4. The same as Fig. 3 but for the model calculations with additional smearing of the anisotropy parameters. The full circles are the ATLAS data from [29].

5 Conclusions

We analyse the event-by-event fluctuations of elliptic and triangular flows in lead-lead collisions at $\sqrt{s_{NN}} = 2.76$ TeV within the HYDJET++ model. To compare the model results with the data the unfolding procedure was employed. Unfolding eliminates to a great extent the non-flow contributions caused by, e.g. decays of resonances, finite event multiplicities and jet fragmentation. These effects cannot be taken away by the rescaling of the distributions. Therefore, for correct comparison of "apples" to "apples" one has to follow the procedure implemented for reconstruction of the experimental data.

The dynamical origin of the flow fluctuations in the model is traced to the correlations between the momenta and coordinates of final particles and the velocities of hadronic fluid elements. Gaussian smearing of the model parameters $\varepsilon(b)$ and $\varepsilon_3(b)$, responsible for spatial asymmetry of the freeze-out hypersurface, has proven to be absolutely necessary for good quantitative description of elliptic and triangular flow fluctuations. These fluctuations can be further linked to the initial-state fluctuations, provided the response of the system is linear.

Acknowledgments

References

[1] L. P. Csernai and H. Stöcker, J. Phys. G **42**, 124001 (2014).

[2] H. G. Ritter and R. Stock, J. Phys. G **42**, 124002 (2014).

[3] J. Jia, J. Phys. G **42**, 124003 (2014).

[4] G. S. Denicol, J. Phys. G **42**, 124004 (2014).

[5] H. Petersen, J. Phys. G **42**, 124005 (2014).

[6] Z. Tang, Nu Xu, K. Zhou, and P. Zhuang, J. Phys. G **42**, 124006 (2014).

[7] R. Snellings, J. Phys. G **42**, 124007 (2014).

[8] S. A. Voloshin and Y. Zhang, Z. Phys. C **70**, 665 (1996).

[9] A. M. Poskanzer and S. A. Voloshin, Phys. Rev. C **58**, 1671 (1998).

[10] S. A. Voloshin, A. M. Poskanzer, and R. Snellings, in *Relativistic Heavy Ion Physics*, Landolt-Börnstein Database Vol. 23, edited by R. Stock (Springer, Berlin, 2010), p.5−54.

[11] E. E. Zabrodin, C. Fuchs, L. V. Bravina, and Amand Faessler, Phys. Lett. B **508**, 184 (2001).

[12] I. P. Lokhtin *et al.*, Comput. Phys. Commun. **180**, 779 (2009).

[13] I. P. Lokhtin *et al.*, Eur. Phys. J. C **72**, 2045 (2012).

[14] L. V. Bravina *et al.*, Eur. Phys. J. C **74**, 2807 (2014).

[15] G. Eyyubova *et al.*, Phys. Rev. C **80**, 064907 (2009).

[16] E. Zabrodin *et al.*, J. Phys. G. **37**, 094060 (2010).

[17] E. Zabrodin, G. Eyyubova, L. Malinina, and L. Bravina, Acta Phys. Polon. B **5**, 349 (2012).

[18] L. Bravina, B. H. Brusheim Johansson, G. Eyyubova, and E. Zabrodin, Phys. Rev. C **87**, 034901 (2013).

[19] E. Zabrodin *et al.*, EPJ Web Confer. **71**, 00142 (2014).

[20] E. Zabrodin *et al.*, EPJ Web Confer. **95**, 03039 (2015).

[21] L. V. Bravina *et al.*, Phys. Rev. C **89**, 024909 (2014).

[22] G. Eyyubova *et al.*, Phys. Rev. C **91**, 064907 (2015).

[23] L. V. Bravina *et al.*, Eur. Phys. J. C **75**, 588 (2015) (arXiv:1509.02692 [hep-ph]).

[24] N. S. Amelin *et al.*, Phys. Rev. C **74**, 064901 (2006).

[25] N. S. Amelin *et al.*, Phys. Rev. C **77**, 014903 (2008).

[26] I. P. Lokhtin and A. M. Snigirev, Eur. Phys. J. C **46**, 211 (2006).

[27] S. A. Voloshin, A. M. Poskanzer, A. Tang, and G. Wang, Phys. Lett. B **659**, 537 (2008).

[28] R. S. Bhalerao and J.-Y. Ollitrault, Phys. Lett. B **641**, 260 (2006).

[29] G. Aad *et al.* (ATLAS Collaboration), JHEP **11**, 183 (2013).

[30] H. Niemi, K. J. Eskola, and R. Paatelainen, arXiv:1505.02677 [hep-ph].

[31] M. Rybczynski and W. Broniowski, arXiv:1510.08242 [nucl-th].

[32] T. Adye, arXiv:1105.1160 [physics.data-an]